

Emulation of quantum correlations by classical dynamics in a spin-1/2 Heisenberg chain

Chaebin Kim^{1,*} and Martin Mourigal^{1,†}

¹*School of Physics, Georgia Institute of Technology, Atlanta, Georgia 30332, USA*

(Dated: March 27, 2025)

We simulate the dynamical spin structure factor (DSSF) $\mathcal{S}(q, \omega)$ of the spin-1/2 Heisenberg antiferromagnetic chain using classical simulations. By employing Landau-Lifshitz Dynamics, we emulate quantum correlations through temperature-dependent corrections, including rescaling of magnetic dipoles and renormalization of exchange interactions. Our results demonstrate that the quantum-equivalent DSSF closely matches Quantum Monte-Carlo calculations for $k_B T/J \gtrsim 1$, capturing the continuum of magnetic excitations observed in neutron scattering measurements. At higher temperatures, our simulations comply with general predictions by De Gennes, where the pinched-oval spectral continuum reflects the uncorrelated paramagnetic fluctuations in the infinite temperature limit. Surprisingly, entanglement witnesses extracted from the quantum-equivalent DSSF mimic quantum calculations across all temperatures, despite relying on classical dynamics. However, classical simulations fail to reproduce higher energy spectral weight from spinon excitations at lower temperatures and struggle to explain the system behavior at intermediate temperatures and magnetic fields. Our approach highlights the potential of classical dynamics to emulate quantum effects even in the most extreme spin systems, with implications for future experimental and theoretical investigations.

The spin-1/2 Heisenberg antiferromagnetic chain is a central model in quantum magnetism, strongly correlated electron systems, and condensed matter physics in general [1]. Its simplicity belies the rich and complex physics it embodies, making it an ideal model for exploring fundamental concepts such as quantum entanglement, deconfined fractional excitations, quantum criticality, and phase transitions. It serves as a theoretical testbed and proving ground for analytical and computational techniques and, perhaps surprisingly, remains of recurring experimental relevance, as it is realized in various quasi-one-dimensional magnetic materials. The ground state of this system can be understood exactly in the zero-temperature limit [2], a regime in which the excitations display a striking quantum phenomenon: the fractionalization of conventional magnons into pairs of spinons [3]. The presence of spinon pairs is associated with a continuum in both zero-temperature [4] and finite-temperature [5, 6] response functions.

In the last decade, continua of magnetic excitations have been evidenced in various magnetic materials by neutron scattering experiments. This has led to rapid developments in numerical techniques to reproduce and explain the physical origin of these continua, which include spin fractionalization, magnon decay, cooperative paramagnetism, and chemical disorder. One such approach, classical dynamics, does not rely on an accurate quantum representation of the ground state and has been surprisingly effective due to its speed and versatility. However, the limits of applicability of classical dynamics are not yet fully understood.

In this Letter, we simulate the dynamical spin structure factor (DSSF) $\mathcal{S}(q, \omega)$ of the quantum (spin-1/2) Heisenberg antiferromagnetic chain (QHAC) using classical simulations [7–13]. We use Landau Lifshitz Dynamics (LLD) to simulate the two-point spin correlations of this paradigmatic model [14, 15] and track their evolution in momentum-energy space as a function of temperature T and uniform magnetic field B . We benchmark our results to existing quantum

calculations previously obtained by Quantum Monte-Carlo (QMC) [6]. Emulating such quantum calculations with classical dynamics relies on the correspondence principle between quantum and classical systems [8, 12, 16, 17] supplemented by two additional temperature-dependent corrections: a self-consistent rescaling of the length of the magnetic dipoles (so-called $\kappa(T)$ rescaling [17]), and a corresponding modification of the antiferromagnetic exchange interaction J (so-called $z(T)$ renormalization [18, 19]) that we derive from the quantum calculations.

Our results are threefold. First, we obtain a quantum-equivalent DSSF that is overall identical to QMC results for $k_B T/J \gtrsim 1$; a regime where the continuum of magnetic excitations observed in neutron scattering measurements [20] is emulated by the highly non-linear spin dynamics of the correlated paramagnet. Second, at lower temperatures $k_B T/J \lesssim 1$, we observe that a large exchange renormalization is necessary to correctly capture the lower bond of the continuum (as expected [21]). In contrast, the classical simulations cannot correctly capture the higher energy spectral weight from spinon excitations [4]. Despite this, entanglement witnesses (EWs) [22–25] extracted from the quantum-equivalent DSSF closely mimic the quantum calculations at all temperatures; a surprising observation given that these simulations rely on a product states between classical dipoles and only emulate quantum effects through simple corrections. Third, we show that our approach to emulating the DSSF of the QHAC fails at intermediate magnetic fields $0 < B < B_{\text{sat}} = 2JS$ for any temperature due to the incommensurate gapless nature of the spin correlations in that regime.

Our model Hamiltonian reads $\hat{\mathcal{H}} = J_a \sum_{\langle i,j \rangle} \hat{\mathbf{S}}_i \cdot \hat{\mathbf{S}}_j - g\mu_B H \sum_i S_i^z$, where J_a is the bare (or atomistic) antiferromagnetic exchange interaction between spin operators $\hat{\mathbf{S}}_i$. This model is approximately realized in a number of quasi-1D $S = 1/2$ compounds including (but not limited to) KCuF_3 [23, 26–28], copper pyrazine dinitrate (CuPzN) [29], $\text{Sr}_n\text{CuO}_{n+1}$ [30, 31], $\text{CuSO}_4 \cdot 5\text{D}_2\text{O}$ [32], and YbAlO_3 [33,

arXiv:2503.19975v1 [cond-mat.str-el] 25 Mar 2025

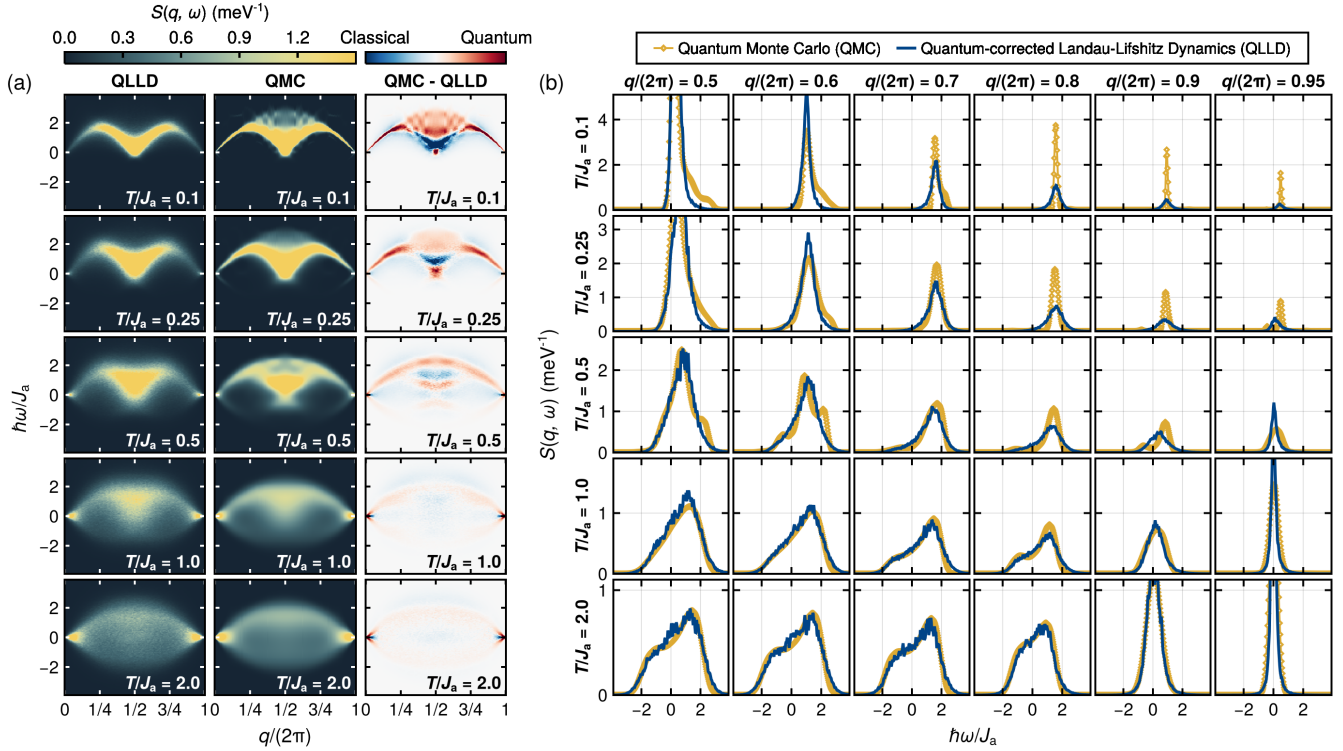


FIG. 1. (a) Dynamical spin structure factor (DSSF) of the quantum Heisenberg antiferromagnetic chain (QHAC) as a function of temperature. The colorplot encodes the diagonal part of the DSSF $\sum_{\alpha} S^{\alpha\alpha}(q, \omega)$ as a function of momentum and energy. The left column is obtained using quantum-corrected Landau-Lifshitz Dynamics (QLLD, this work), while the center column corresponds to Quantum Monte Carlo results from Ref. 6. The left column is a plot of the difference between these two approaches. (b) A comparison between QLLD (blue lines) and QMC (gold lines) is made through the energy dependence of the DSSF at constant momenta, as indicated at the top of the column. The temperature is shown in each row. The dynamical structure factor is calculated in units of $J_a^{-1} = \text{meV}^{-1}$.

34]. These compounds span remarkably diverse chemical families and exchange interaction scales; as a result, a broad range of values for $k_B T/J_a$ and $g\mu_B H/J_a$ are accessible to detailed experimental investigations, especially using neutron scattering. High-fidelity theoretical predictions for the DSSF of this model have also been obtained using the Bethe Ansatz in the zero-temperature limit [4, 35], as well as Quantum Monte-Carlo [5, 6] and Matrix Product States techniques [23, 24, 36, 37] in various regimes.

To calculate the DSSF with classical dynamics, we describe possible spin states as product states $|\Omega\rangle = \otimes_i |\Omega_i\rangle$, where $|\Omega_i\rangle$ is a coherent state representing the $S = 1/2$ dipole moment at site i using a classical vector $\Omega_i \equiv \langle \Omega_i | \hat{S}_i | \Omega_i \rangle$. The space-time dynamics of the classical dipoles are sampled from thermal equilibrium spin configurations evolving according to the Landau-Lifshitz equation of motion (LLD), as implemented in the SUNNY.JL [38] package [see Supplementary Information for details of our calculations]. Because spin configurations are sampled with Boltzmann statistics, the classical DSSF must be corrected to emulate a quantum response at low temperatures. In the zero-temperature limit, the correction factor, $\hbar\omega/k_B T \times [1 - \exp(-\hbar\omega/k_B T)]^{-1}$, stems from the exact equivalence/correspondence between quantum and clas-

sical harmonic oscillators [8, 12, 13, 16, 17]. This correspondence is not exact at finite temperatures, given the non-linear nature of the classical dynamics.

To progress, we implement two ad-hoc corrections. First, the norm of each classical dipole is scaled to $|\Omega_i(T)| = \kappa(T)S$, with a rescaling factor $\kappa(T)$ calculated self-consistently such that the corrected DSSF fulfills the zeroth-moment sum-rule $\sum_{\alpha} \iint S^{\alpha\alpha}(q, \omega) d\omega dq = S(S+1)$ at every simulation temperature [17]. Second, the exchange interaction itself is renormalized by a factor $z(T)$ [18, 19] to match the energy bandwidth of the true quantum DSSF previously obtained by QMC [6]. This matching is achieved by a least-squares fitting between our DSSF calculations and QMC, with $z(T)$ as a fitting parameter [see Supplementary Information]. While these two corrections appear together in the classical Hamiltonian \mathcal{H}_{cl} controlling the dynamics, effectively rescaling the exchange interaction as $J_a \rightarrow J_a z \kappa^2(T)$, only $\kappa(T)$ impacts the spectral sum-rule and thus both corrections play distinct roles, as we will show below. We refer to the resulting simulations as quantum-corrected Landau-Lifshitz dynamics (QLLD).

In Fig. 1, we compare the momentum- and energy-dependence of the DSSF calculated with QLLD to the QMC

results from Ref. 6. We focus on energies up to $\hbar\omega_{\max} = \pi J_a$ bounded by the upper branch of the two-spinon continuum [35]. In the zero-temperature limit, this energy band is known to contain most of the spectral weight [4]. In the high-temperature limit, which we define here as $k_B T/J_a \gtrsim 1$, the dominant features of the DSSF are virtually identical between QLLD and QMC as shown on two-dimensional spectral plots [Fig. 1(a)-right/center] and constant-momentum line cuts [Fig. 1(b)]. The pinched-oval spectral continuum, which closely resembles recent experimental and numerical results on YbAlO_3 [34] where it was associated with high-temperature quantum coherence of spinons, is accurately emulated by the classical dynamics of paramagnetic spins upon simple $\kappa(T)$ and $z(T)$ corrections [See Supplementary Information for detailed plots of the uncorrected DSSF]. As we argue below, the shape of this paramagnetic continuum is universal for Heisenberg paramagnets and reflects that total magnetization is a conserved quantity. We nonetheless observe two small deviations between QLLD and QMC in this temperature regime, apparent in both line cuts [Fig. 1(b)] and subtraction spectral plots [Fig. 1(a)-left]. First, the drop in spectral intensity at higher energies appears sharper in QMC, which we hypothesize originates from details of the analytical continuation used in Ref. 6. Second, in the vicinity of the zone center, the energy width of the DSSF at fixed momentum $q \rightarrow 0, 2\pi$ appears broader in QMC compared to QLLD; this is the only genuine deficiency of the QLLD approach above $k_B T/J_a \gtrsim 1$.

At lower temperatures, $k_B T/J_a \lesssim 1$, deviations between QLLD and QMC become more significant, as is apparent from difference spectral plots [Fig. 1(a)-right] and line cuts [Fig. 1(b)]. The strong signal at the lower boundary of the excitation continuum is well reproduced by QLLD, proving the effectiveness of our $z(T)$ renormalization approach. However, QLLD cannot explain the enhanced spectral weight at higher energies — the hallmark of a multi-spinon continuum — because of the classical nature of the underlying degrees of freedom and dynamics. This is particularly clear for $k_B T/J_a = 0.1$ and $k_B T/J_a = 0.25$, from the broad red area between $0.4 \leq q/(2\pi) \leq 0.6$ in Fig. 1(a)-right which signals the failure of QLLD to produce an asymmetric energy continuum. Second, QLLD produces a spectral distribution considerably broader than QMC near the Brillouin zone center. This effect is particularly striking in the line cuts of Fig. 1(b), which shows that the momentum-dependent peak broadening and suppression in QLLD is much more pronounced than that of QMC. We ascribe this discrepancy to the incapacity of QLLD to capture the coherent propagation of spinon excitations pointed out in Ref. 34.

We now turn to details of our exchange renormalization procedure, which yields a temperature-dependent exchange interaction $J(T) = z(T)J_a$ reflecting a genuine quantum effect not captured by the classical dynamics and necessary to match the overall energy scale. In Fig. 2(a), we empirically compare the temperature dependence of $z(T)$ and $\kappa(T)$. Both quantities display an exponential-like behavior:

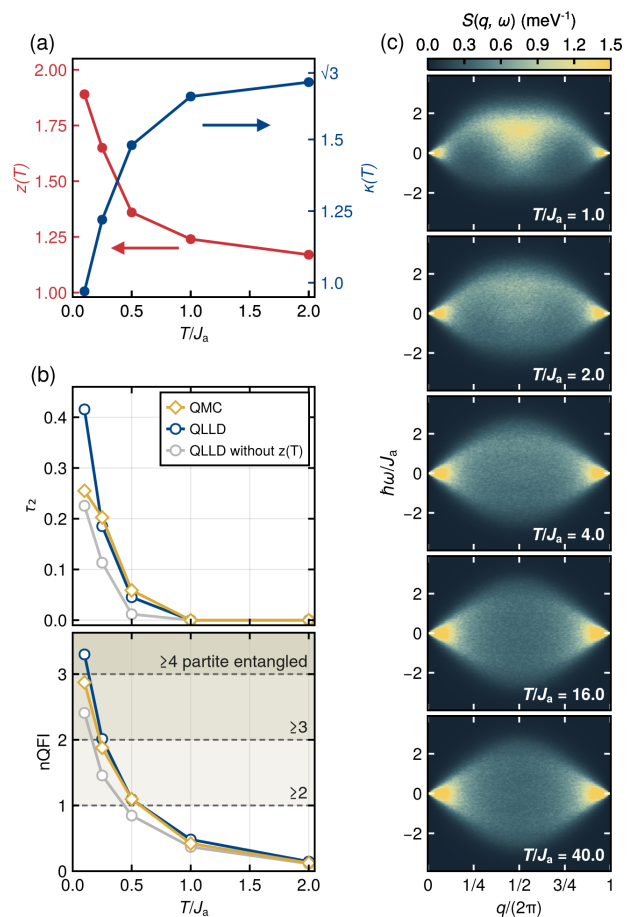


FIG. 2. (a) Temperature dependence of the exchange renormalization factor $z(T)$ (red line) and moment rescaling factor $\kappa(T)$ (blue line) extracted from QLLD simulations with $z(T)$ fitted from QMC results. The y-scale corresponding to each quantity is highlighted with corresponding colors and arrows. (b) Temperature dependence of entanglement witnesses (two-tangle and Quantum Fisher Information) extracted from QMC (gold lines) and LLD simulations, the latter with (blue lines) and without (gray lines) $z(T)$ -renormalization. The upper panel shows the temperature dependence of the two-tangle and the bottom panel shows the temperature dependence of the normalized quantum Fisher information. Grey dashed lines indicate the integer number of normalized QFI, which guarantees the lower bound of the $(n+1)$ multipartite entanglement. (c) High-temperature simulations of the DSSF using QLLD. For temperatures higher than $k_B T/J_a = 2$, we used $z(T) = 1.14$ and $\kappa(T) = \sqrt{3}$ from Fig. 2(a).

the moment rescaling $\kappa(T)$ increases with temperature from $\kappa(T \rightarrow 0) = 1$ to $\kappa(T \rightarrow \infty) = \sqrt{S(S+1)}/\sqrt{S^2} = \sqrt{3}$ as needed from general principles; the exchange renormalization $z(T)$ appears anti-correlated with this behavior and increases with decreasing temperature from $z(T) = 1.14$ for $k_B T/J_a = 2$ to $z(T) \approx 1.9$ for $k_B T/J_a = 0.1$. This behavior is consistent with general expectations but deviates from naive expectations of $z(T \rightarrow 0) = \pi/2$, consistent with Des Cloizeaux-Person [21, 32] and $z(T \rightarrow \infty) = 1$. Interestingly, we observe that the product $z(T) \cdot \kappa(T) \approx 2$ is a constant

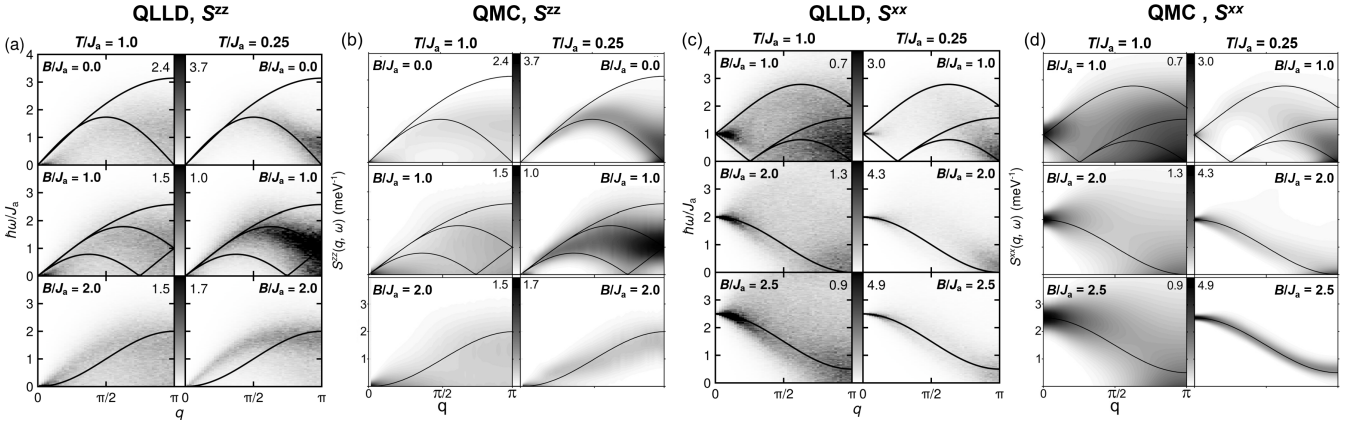


FIG. 3. Field and temperature dependence of DSSF by QMC and QLLD. (a),(b) Longitudinal DSSF $S^{zz}(q, \omega)$ of QLLD and QMC method, respectively. For the $B/J_a < 2$, white lines indicate the excitation boundary from the Muller ansatz at zero temperature. For the critical field $B/J_a = 2$, dispersion becomes $\omega(q) = 1 - \cos(q)$. (c),(d) Transverse DSSF $S^{xx}(q, \omega)$ of QLLD and QMC method, respectively. The temperature is shown at the top of the column and the magnetic field is given in each box. The QMC results are from [6].

regardless of the temperature, which reflects that the energy-distribution of spectral weight is proportional to $J(T) \cdot |\Omega(T)|$.

To better understand how our QLLD simulations emulate the DSSF of the QHAC, we extend our examination to entanglement witnesses [22–25] which have recently been proposed as a general protocol to certify the presence of bipartite and multipartite quantum entanglement in spin systems through the momentum- and energy-dependence of the DSSF. These approaches have been discussed extensively for the QHAC in the context of experimental data for KCuF_3 and YbAlO_3 , and numerical tensor network results [23, 24, 34, 36, 37]. Here, we test how classical dynamics compares with quantum calculations for two entanglement witnesses (EWs): the two-tangle (τ_2) characterizing the total entanglement carried by pairwise correlations, and the normalized quantum fisher information (nQFI), which can be interpreted as the lower bound of the multipartite entanglement [See Supplementary Information for definitions]. Fig. 2(b) shows $\tau_2(T)$ and nQFI(T) extracted from three different numerical datasets: QMC, QLLD, and QLLD without $z(T)$ renormalization. The overall trend and values for these EWs are similar across all three approaches and resemble previous results. Surprisingly, we find that the DSSF calculated using classical dynamics — even without exchange renormalization — can produce above threshold values for τ_2 and nQFI for $k_B T/J_a < 1$; this is naively consistent with the presence of multipartite entanglement even though the underlying simulation relies on purely precessional spin dynamics. Because the DSSF simulated by QLLD closely resembles the quantum result, classical dynamics can emulate the value of entanglement witnesses and mimic the presence of quantum entanglement. We further remark that the temperature regime for which significant differences exist between QMC and QLLD [$k_B T/J_a < 1$, Fig. 1(a)] is correlated to EWs rising above threshold values for pair and multipartite entanglement [Fig. 2(b)]. From these two observations, we postulate EWs

might be an adequate self-consistent tool to assess if and when quantum-corrected classical dynamic simulations of the DSSF become inaccurate.

We now turn to the high-temperature regime $k_B T/J_a > 2$, for which we have extended QLLD simulations up to $k_B T/J_a = 40$ [Fig. 2(c)]. Classical dynamics accurately represent the DSSF in the $T \rightarrow \infty$ limit. The pinched-oval gapless spectral continuum observed for $k_B T/J_a = 4, 16$, and 40, is thus the hallmark of uncorrelated paramagnetic fluctuations. As was pointed out by De Gennes in 1958 [39], this behavior can be understood from general principles and is readily captured by classical dynamics for other Heisenberg spin systems [40]. For the QHAC in the limit of $q \rightarrow 0$, the Fourier transformed spin operator $\hat{S}_q^z = 1/\sqrt{L} \sum_j \exp(iqr_j) \hat{S}_j^z$ commutes with the Hamiltonian at any temperature, $[\hat{S}_{q=0}^z, \mathcal{H}]_T = 0$, as the total magnetization $\hat{M}_{\text{tot}}^z = \sqrt{L} \hat{S}_{q=0}^z$ is conserved. Thus, the DSSF $S^{zz}(q = 0, \omega, T) = \langle [\hat{M}_{\text{tot}}^z]^2 \rangle / L \delta(\omega)$ is purely elastic in the $q \rightarrow 0$ limit. This argument can be extended from the Brillouin zone center by considering the spectral weight distribution’s second moment (or variance), $\sigma^2(q, T)$. Clearly, as discussed above, $\sigma(q \rightarrow 0, T) = 0$ for any temperature. For finite momentum, the variance can only be approximated in the infinite temperature limit by considering the system’s translational, inversion, and rotational invariance. This yields $\sigma^2(q, T \rightarrow \infty) = 2J_a(1 - \cos q)$ [39] for the QHAC. This readily explains the pinched-oval spectral distribution (which we propose to call the “De Gennes continuum”) observed in our QLLD simulations and recent experiments on YbAlO_3 [34]. This is a universal feature of diffusive precessional spin dynamics [9, 41] in an uncorrelated Heisenberg paramagnet.

Finally, we remark on an important limitation of our current implementation of classical dynamics to model the QHAC, which arises by considering the dynamics in an applied magnetic field. We use QLLD to simulate the transverse and longitudinal contributions to the DSSF at finite temperature and

finite field and compare our results with QMC [6]. Results in applied magnetic fields of $B/J_a = g\mu_B H/J_a = 1.0, 2.0, 2.5$ (the saturation field of the quantum model is $B_s/J_a = 2.0$) are shown for $k_B T/J_a = 0.25$ and 1.0 [longitudinal \mathcal{S}^{zz} , Fig. 3(a-b); transverse \mathcal{S}^{xx} , Fig. 3(c-d)]. In the low-temperature limit, it is well known that incommensurate magnetic correlations develop even for realistic systems [29, 33]. This phenomenon can be pictured in the language of fermionic spinons as originating from a shift in chemical potential away from half-filling, yielding low-energy excitations incommensurate with the crystallographic cell. While QMC captures these correlations, QLLD fails to reproduce them, see *e.g.* $B/J_a = 1$ at $k_B T/J_a = 0.25$. Perhaps more surprisingly, it is also difficult for QLLD simulations to reproduce the DSSF in the vicinity of the saturation field itself, see *e.g.* $B/J_a = 2$ at $k_B T/J_a = 0.25$, where the magnetization curve of the system changes rapidly [42, 43] and cannot be captured by classical simulations sampling from a Boltzmann distribution. To address this problem, rescaling the magnetic field scale to emulate the correct quantum magnetization curve seems appealing, especially considering the success of our $z(T)$ renormalization scheme. However, simulations need to correctly capture the energy of the $q = 0$ Larmor mode at $\hbar\omega = B$ [Fig. 3(c)]. This feature, which corresponds to the uniform precession of spins in the magnetic field, dominates the transverse structure factor and is *immune* to quantum corrections [44]. The competition between these effects makes it difficult to devise a simple approach to correct the QLLD in applied magnetic fields, and we leave this to future work.

Our work reinforces the emerging consensus that non-linear classical dynamics can often faithfully emulate the DSSF of quantum spins at finite but small temperatures [19, 45–47]. This point was recently demonstrated in a spin-1/2 ladder system with a small gap [48], and it is remarkable that this approach, with some simple quantum corrections, continues to work down to $k_B T/J_a \approx 1$ in the extreme case of gapless correlations in the quantum Heisenberg antiferromagnetic chain. QLLD simulations thus provide a likely universal approach to extract model Hamiltonians from inelastic neutron scattering data, offering a complementary method to diffuse scattering [49] and saturated field measurements [32] for systems where the saturation field is too high or reached only asymptotically. Despite the clear quantum effects that classical dynamics cannot capture, especially at low temperatures, this approach *can* EWs. This result highlights a limit to their sensitivity but shows they can serve as a diagnostic tool to identify the failure of classical simulations. Finally, as classical dynamics yields the exact DSSF in the high-temperature limit for any quantum spin system, our work underscores the connection between continua of fractional excitations at low temperatures and paramagnetic scattering at high temperatures in Heisenberg spin systems.

This work was supported by the US Department of Energy, Office of Science, Basic Energy Sciences, Materials Sciences and Engineering Division under award DE-SC-0018660. The authors are especially grateful to Prof. Wolfram Brenig for

sharing their QMC data and indebted to Prof. Cristian Batista for his numerous insights. The authors also thank Dr. David Dalhobom and Pyeongjae Park for helpful discussions about $\kappa(T)$ rescaling.

* ckim706@gatech.edu

† mourigal@gatech.edu

- [1] T. Giamarchi, *Quantum physics in one dimension*, 1st ed., International Series of Monographs on Physics (Oxford University Press., Oxford, U.K., [2003]).
- [2] H. Bethe, Zur theorie der metalle, *Zeitschrift für Physik* **71**, 205 (1931).
- [3] L. Faddeev and L. Takhtajan, What is the spin of a spin wave?, *Physics Letters A* **85**, 375 (1981).
- [4] J.-S. Caux and R. Hagemans, The four-spinon dynamical structure factor of the heisenberg chain, *Journal of Statistical Mechanics: Theory and Experiment* **2006**, P12013 (2006).
- [5] O. A. Starykh, A. W. Sandvik, and R. R. P. Singh, Dynamics of the spin- heisenberg chain at intermediate temperatures, *Phys. Rev. B* **55**, 14953 (1997).
- [6] S. Grossjohann and W. Brenig, Spin dynamics of the antiferromagnetic spin-1/2 chain at finite magnetic fields and intermediate temperatures, *Physical Review B* **79**, 094409 (2009).
- [7] A. Keren, Dynamical simulation of spins on kagomé and square lattices, *Phys. Rev. Lett.* **72**, 3254 (1994).
- [8] T. Huberman, D. A. Tennant, R. A. Cowley, R. Coldea, and C. D. Frost, A study of the quantum classical crossover in the spin dynamics of the 2d $s = 5/2$ antiferromagnet rb2mnf4: neutron scattering, computer simulations and analytic theories, *Journal of Statistical Mechanics: Theory and Experiment* **2008**, P05017 (2008).
- [9] P. H. Conlon and J. T. Chalker, Spin dynamics in pyrochlore heisenberg antiferromagnets, *Phys. Rev. Lett.* **102**, 237206 (2009).
- [10] M. Taillefumier, J. Robert, C. L. Henley, R. Moessner, and B. Canals, Semiclassical spin dynamics of the antiferromagnetic heisenberg model on the kagome lattice, *Phys. Rev. B* **90**, 064419 (2014).
- [11] A. M. Samarakoon, A. Banerjee, S.-S. Zhang, Y. Kamiya, S. E. Nagler, D. A. Tennant, S.-H. Lee, and C. D. Batista, Comprehensive study of the dynamics of a classical kitaev spin liquid, *Phys. Rev. B* **96**, 134408 (2017).
- [12] S. Zhang, H. J. Changlani, K. W. Plumb, O. Tchernyshyov, and R. Moessner, Dynamical structure factor of the three-dimensional quantum spin liquid candidate nacani₂f₇, *Phys. Rev. Lett.* **122**, 167203 (2019).
- [13] K. Remund, R. Pohle, Y. Akagi, J. Romhányi, and N. Shannon, Semi-classical simulation of spin-1 magnets, *Phys. Rev. Res.* **4**, 033106 (2022).
- [14] D. Dahlbom, C. Miles, H. Zhang, C. D. Batista, and K. Barros, Langevin dynamics of generalized spins as $su(n)$ coherent states, *Phys. Rev. B* **106**, 235154 (2022).
- [15] D. Dahlbom, H. Zhang, C. Miles, X. Bai, C. D. Batista, and K. Barros, Geometric integration of classical spin dynamics via a mean-field schrödinger equation, *Phys. Rev. B* **106**, 054423 (2022).
- [16] P. Schofield, Space-time correlation function formalism for slow neutron scattering, *Phys. Rev. Lett.* **4**, 239 (1960).
- [17] D. Dahlbom, F. T. Brooks, M. S. Wilson, S. Chi, A. I. Kolesnikov, M. B. Stone, H. Cao, Y.-W. Li, K. Barros,

- M. Mourigal, C. D. Batista, and X. Bai, Quantum-to-classical crossover in generalized spin systems: Temperature-dependent spin dynamics of FeI₂, *Physical Review B* **109**, 014427 (2024).
- [18] C. M. Canali and S. M. Girvin, Theory of raman scattering in layered cuprate materials, *Phys. Rev. B* **45**, 7127 (1992).
- [19] P. Park, G. Sala, D. M. Pajerowski, A. F. May, J. A. Kolopus, D. Dahlbom, M. B. Stone, G. B. Halász, and A. D. Christianson, Quantum and classical spin dynamics across temperature scales in the $S = 1/2$ heisenberg antiferromagnet, *Physical Review Research* **6**, 033184 (2024).
- [20] Measurements at typical momentum and energy resolution.
- [21] J. des Cloizeaux and J. J. Pearson, Spin-wave spectrum of the antiferromagnetic linear chain, *Physical Review* **128**, 2131 (1962).
- [22] P. Hauke, M. Heyl, L. Tagliacozzo, and P. Zoller, Measuring multipartite entanglement through dynamic susceptibilities, *Nature Physics* **12**, 778 (2016).
- [23] A. Scheie, P. Laurell, A. M. Samarakoon, B. Lake, S. E. Nagler, G. E. Granroth, S. Okamoto, G. Alvarez, and D. A. Tennant, Witnessing entanglement in quantum magnets using neutron scattering, *Physical Review B* **103**, 224434 (2021).
- [24] P. Laurell, A. Scheie, C. J. Mukherjee, M. M. Koza, M. Enderle, Z. Tylczynski, S. Okamoto, R. Coldea, D. A. Tennant, and G. Alvarez, Quantifying and controlling entanglement in the quantum magnet Cs₂CoCl₄, *Physical Review Letters* **127**, 037201 (2021).
- [25] P. Laurell, A. Scheie, E. Dagotto, and D. A. Tennant, Witnessing entanglement and quantum correlations in condensed matter: A review, *arXiv* (2024).
- [26] D. A. Tennant, T. G. Perring, R. A. Cowley, and S. E. Nagler, Unbound spinons in the $s=1/2$ antiferromagnetic chain kcuF₃, *Phys. Rev. Lett.* **70**, 4003 (1993).
- [27] B. Lake, D. A. Tennant, C. D. Frost, and S. E. Nagler, Quantum criticality and universal scaling of a quantum antiferromagnet, *Nature Materials* **4**, 329 (2005).
- [28] B. Lake, D. A. Tennant, J.-S. Caux, T. Barthel, U. Schollwöck, S. E. Nagler, and C. D. Frost, Multispinon continua at zero and finite temperature in a near-ideal heisenberg chain, *Phys. Rev. Lett.* **111**, 137205 (2013).
- [29] M. B. Stone, D. H. Reich, C. Broholm, K. Lefmann, C. Rischel, C. P. Landee, and M. M. Turnbull, Extended quantum critical phase in a magnetized spin- $\frac{1}{2}$ antiferromagnetic chain, *Phys. Rev. Lett.* **91**, 037205 (2003).
- [30] I. A. Zaliznyak, H. Woo, T. G. Perring, C. L. Broholm, C. D. Frost, and H. Takagi, Spinons in the strongly correlated copper oxide chains in srCuO₂, *Phys. Rev. Lett.* **93**, 087202 (2004).
- [31] J. Schlappa, K. Wohlfeld, K. J. Zhou, M. Mourigal, M. W. Haverkort, V. N. Strocov, L. Hozoi, C. Monney, S. Nishimoto, S. Singh, A. Revcolevschi, J.-S. Caux, L. Patthey, H. M. Rønnow, J. van den Brink, and T. Schmitt, Spin-orbital separation in the quasi-one-dimensional mott insulator sr₂cuo₃, *Nature* **485**, 82 (2012).
- [32] M. Mourigal, M. Enderle, A. Klöpperpieper, J.-S. Caux, A. Stunault, and H. M. Rønnow, Fractional spinon excitations in the quantum heisenberg antiferromagnetic chain, *Nature Physics* **9**, 435 (2013).
- [33] L. S. Wu, S. E. Nikitin, Z. Wang, W. Zhu, C. D. Batista, A. M. Tsvelik, A. M. Samarakoon, D. A. Tennant, M. Brando, L. Vasylechko, M. Frontzek, A. T. Savici, G. Sala, G. Ehlers, A. D. Christianson, M. D. Lumsden, and A. Podlesnyak, Tomonaga-luttinger liquid behavior and spinon confinement in ybalo₃, *Nature Communications* **10**, 698 (2019).
- [34] L. L. Kish, A. Weichselbaum, D. M. Pajerowski, A. T. Savici, A. Podlesnyak, L. Vasylechko, A. Tsvelik, R. Konik, and I. A. Zaliznyak, High-temperature quantum coherence of spinons in a rare-earth spin chain (2024), [arXiv:2406.16753](https://arxiv.org/abs/2406.16753).
- [35] M. Karbach, G. Müller, A. H. Bougourzi, A. Fledderjohann, and K.-H. Mütter, Two-spinon dynamic structure factor of the one-dimensional $s=$ heisenberg antiferromagnet, *Phys. Rev. B* **55**, 12510 (1997).
- [36] M. Dupont and J. E. Moore, Universal spin dynamics in infinite-temperature one-dimensional quantum magnets, *Phys. Rev. B* **101**, 121106 (2020).
- [37] V. Menon, N. E. Sherman, M. Dupont, A. O. Scheie, D. A. Tennant, and J. E. Moore, Multipartite entanglement in the one-dimensional spin- $\frac{1}{2}$ heisenberg antiferromagnet, *Phys. Rev. B* **107**, 054422 (2023).
- [38] Su(n)ny, spin dynamics and generalization to su(n) coherent states, <https://github.com/SunnySuite/Sunny.jl>.
- [39] P. De Gennes, Inelastic magnetic scattering of neutrons at high temperatures, *Journal of Physics and Chemistry of Solids* **4**, 223 (1958).
- [40] A. Bunker, K. Chen, and D. P. Landau, Critical dynamics of the body-centered-cubic classical heisenberg antiferromagnet, *Phys. Rev. B* **54**, 9259 (1996).
- [41] S. Grossjohann and W. Brenig, Hydrodynamic limit for the spin dynamics of the heisenberg chain from quantum monte carlo calculations, *Physical Review B* **81**, 012404 (2010).
- [42] J. C. Bonner and M. E. Fisher, Linear magnetic chains with anisotropic coupling, *Phys. Rev.* **135**, A640 (1964).
- [43] J. B. Parkinson and J. C. Bonner, Spin chains in a field: Crossover from quantum to classical behavior, *Phys. Rev. B* **32**, 4703 (1985).
- [44] M. Oshikawa and I. Affleck, Electron spin resonance in $s = \frac{1}{2}$ antiferromagnetic chains, *Phys. Rev. B* **65**, 134410 (2002).
- [45] A. M. Samarakoon, G. Wachtel, Y. Yamaji, D. A. Tennant, C. D. Batista, and Y. B. Kim, Classical and quantum spin dynamics of the honeycomb Γ model, *Phys. Rev. B* **98**, 045121 (2018).
- [46] W. Steinhart, Z. Shi, A. Samarakoon, S. Dissanayake, D. Graf, Y. Liu, W. Zhu, C. Marjerrison, C. D. Batista, and S. Haravifard, Constraining the parameter space of a quantum spin liquid candidate in applied field with iterative optimization, *Phys. Rev. Res.* **3**, 033050 (2021).
- [47] O. Franke, D. Călugăru, A. Nunnenkamp, and J. Knolle, Thermal spin dynamics of kitaev magnets: Scattering continua and magnetic field induced phases within a stochastic semiclassical approach, *Phys. Rev. B* **106**, 174428 (2022).
- [48] D. A. Dahlbom, J. Thomas, S. Johnston, K. Barros, and C. D. Batista, Classical dynamics of the antiferromagnetic heisenberg $s = \frac{1}{2}$ spin ladder, *Phys. Rev. B* **110**, 104403 (2024).
- [49] J. A. M. Paddison and A. L. Goodwin, Empirical magnetic structure solution of frustrated spin systems, *Phys. Rev. Lett.* **108**, 017204 (2012).
- [50] R. Pohle, H. Yan, and N. Shannon, Theory of ca₁₀cr₇o₂₈ as a bilayer breathing-kagome magnet: Classical thermodynamics and semiclassical dynamics, *Phys. Rev. B* **104**, 024426 (2021).
- [51] B. Skubic, J. Hellsvik, L. Nordström, and O. Eriksson, A method for atomistic spin dynamics simulations: implementation and examples, *Journal of Physics: Condensed Matter* **20**, 315203 (2008).
- [52] G. Müller, H. Thomas, H. Beck, and J. C. Bonner, Quantum spin dynamics of the antiferromagnetic linear chain in zero and nonzero magnetic field, *Physical Review B* **24**, 1429 (1981).

SUPPLEMENTAL INFORMATION

1. CALCULATION OF THE QUANTUM-EQUIVALENT DYNAMICAL STRUCTURE FACTOR AND SPIN RE-SCALING

The quantum Hamiltonian of the system, $\hat{\mathcal{H}}_Q = J_a \sum_{\langle i,j \rangle} \hat{\mathbf{S}}_i \cdot \hat{\mathbf{S}}_j - g\mu_B H \sum_i \hat{S}_i^z$, is simulated by a classical theory with the following properties; possible spin states are restricted to product states $|\mathbf{\Omega}\rangle = \otimes_i |\Omega_i\rangle$, where $|\Omega_i\rangle$ is a SU(2) coherent state representing the $S = 1/2$ moment at site i ; the dynamics of the resulting dipoles is generated by the classical Hamiltonian $\mathcal{H}_{cl} = J \sum_{\langle i,j \rangle} \mathbf{\Omega}_i \cdot \mathbf{\Omega}_j - g\mu_B H \sum_i \Omega_i^z$ with classical dipoles $\mathbf{\Omega}_i \equiv \langle \Omega_i | \hat{\mathbf{S}}_i | \Omega_i \rangle$ evolving according to the Landau-Lifshitz equation of motion $\dot{\mathbf{\Omega}}_i(t) = d\mathcal{H}_{cl}/d\mathbf{\Omega}_i(t) \times \mathbf{\Omega}_i(t)$. To emulate the quantum dynamical spin structure factor, we define two distinct temperature-dependent correction factors. First, the exchange interaction $J \equiv z(T)J_a$ employed in our classical simulations is defined in terms of the bare exchange interaction J_a of the quantum Hamiltonian $\hat{\mathcal{H}}_Q$ and a temperature-dependent exchange renormalization factor $z(T)$. The renormalization factor $z(T)$ is a priori unknown but can be inferred from corresponding quantum calculations, if available. Second, the length of the classical magnetic dipoles is re-scaled by a temperature-dependent factor $\kappa(T)$ such that $|\mathbf{\Omega}_i(T)| \equiv \kappa(T)S$. One way to determine the scaling factor $\kappa(T)$ is to ensure the dynamical spin structure factor fulfills the zeroth-moment quantum sum-rule at every simulation temperature [17]. All the classical dynamics simulations were performed using the SUNNY.JL package for a one-dimensional Heisenberg chain with $N = 100$ sites and periodic boundary conditions [38]. The time trajectory of each spin was traced with a time step of $\Delta t = 0.025/J_a$. Thermalized spin configurations were cooled from random configurations ($T \rightarrow \infty$) using (dissipative) Langevin dynamics with 10,000 time steps and a dimensionless damping parameter of 0.1 representing the coupling to the thermal bath [14]. During thermalization we kept $\kappa(T) = 1$. After thermalization, the spin length was self-consistently scaled by $\kappa(T)$ and the dissipationless spin trajectories obtained using Landau Lifshitz dynamics over 5,000 time steps. In the end, 100 equilibrium space-time spin configurations were sampled, each separated by 3,000 Langevin timesteps to achieve de-correlation. The classical dynamical spin structure factor (DSSF) was obtained from these spin configurations as

$$\mathcal{S}_{cl}^{\alpha\beta}(\mathbf{q}, \omega) = \int dt e^{-i\omega t} \langle \Omega_{\mathbf{q}}^\alpha(t) \Omega_{-\mathbf{q}}^\beta(0) \rangle_T \quad (\text{S1})$$

after performing a lattice Fourier transform of the trajectories and where $\alpha = x, y, z$. The quantum-equivalent [16] DSSF is then obtained using the energy- and temperature-dependent correction [12],

$$\mathcal{S}_Q^{\alpha\beta}(\mathbf{q}, \omega) = \text{sgn}(\omega) \frac{\hbar\omega}{k_B T} \frac{1}{1 - e^{-\hbar\omega/k_B T}} \mathcal{S}_{cl}^{\alpha\beta}(\mathbf{q}, \omega), \quad (\text{S2})$$

with a spin rescaling factor $\kappa(T)$ determined such the DSSF fullfills the zeroth-moment quantum sum rule at every temperature,

$$\sum_{\alpha} \int_{-\infty}^{\infty} d\omega \int d\mathbf{q} \mathcal{S}_Q^{\alpha\alpha}(q, \omega) = NS(S+1). \quad (\text{S3})$$

2. DETERMINATION OF THE TEMPERATURE-DEPENDENT EXCHANGE RENORMALIZATION

The determination of the exchange renormalization factor $z(T)$ for each temperature was done by minimizing the χ^2 between the quantum DSSF obtained by Quantum Monte-Carlo [41] and the quantum-equivalent DSSF, Eq. S2, obtained from Landau Lifshitz Dynamics (LLD). The loss function χ^2 is defined as,

$$\chi^2 = \sum_{i,j} [\mathcal{S}_{QMC}(q_i, \omega_j) - \mathcal{S}_{QLLD}(q_i, \omega_j)]^2, \quad (\text{S4})$$

where (q_i, ω_j) is the momentum-energy grid of the DSSF from QMC simulations, with the result of LLD simulations interpolated on the same grid. The spin-space index α is omitted in the above given that the model displays spin-space isotropy at all temperatures in both QMC and LLD simulations. The behavior of the DSSF from LLD simulations is complicated in the vicinity of the elastic signal due to the stochastic nature of the sampled spin configurations. When minimizing Eq. S4, we find that a global minimum is much better defined in the high temperature regimes ($T/J_a > 1$) when the quasi-elastic signal, corresponding to $|\hbar\omega/J_a| < 0.1$, is masked, see Fig. S1(a-e). The resulting χ^2 gives a well-defined global minimum for each temperature, with an exponential increase of $z(T) = J(T)/J_a$ with decreasing temperature, see Fig. S1(f).

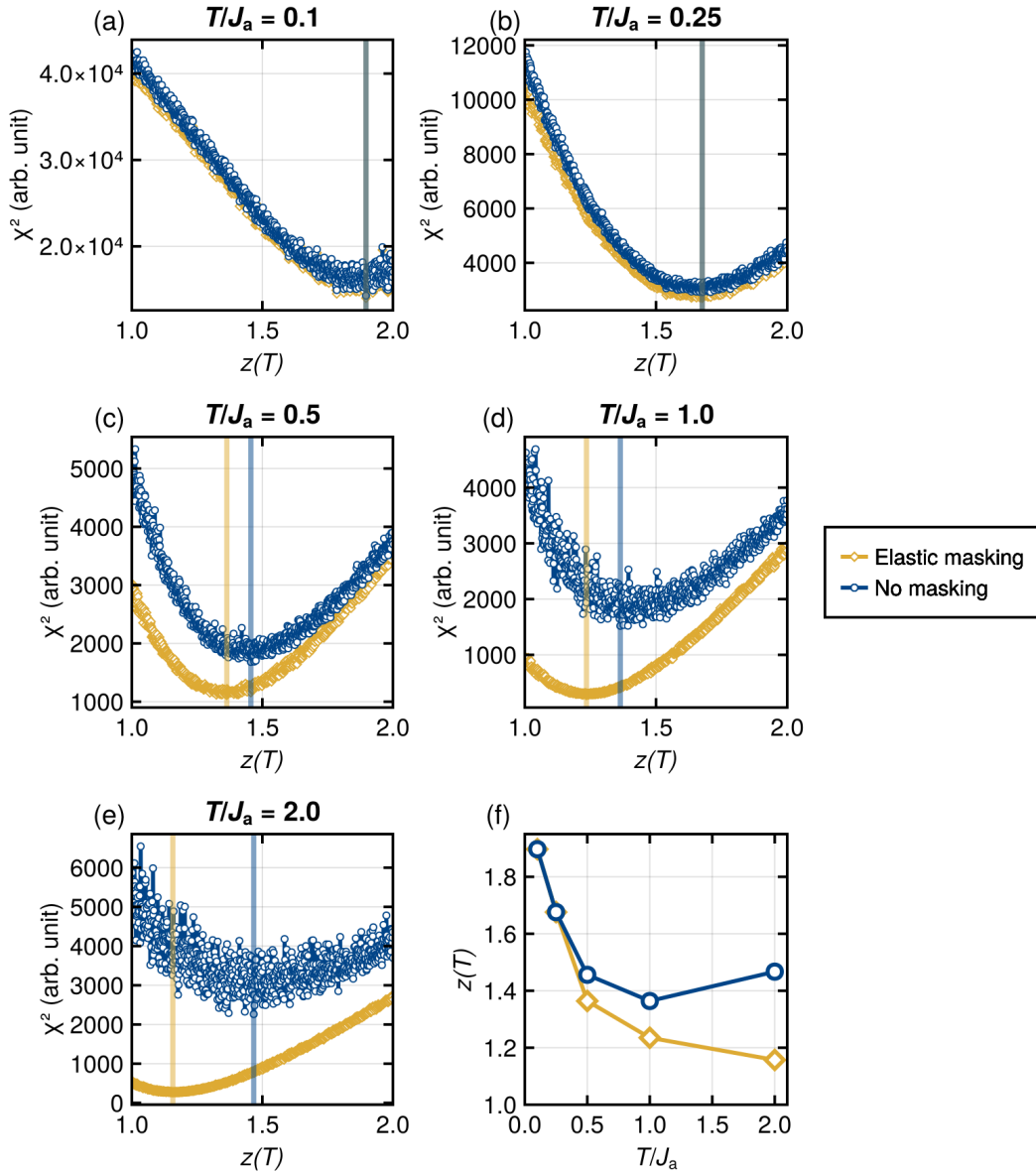


FIG. S1. Determination of $z(T)$ by direct comparison between QMC and LLD simulations. (a)-(e) χ^2 of Eq. S4 for each simulation temperature, where the color-coded vertical lines indicate the global minimum of χ^2 resulting from the minimization. (f) Temperature dependence of the resulting $z(T)$. The blue lines show a comparison without a masking of the elastic energy. Gold lines indicate the comparison with elastic energy masking ($|\hbar\omega/J_a| < 0.1$).

3. ENTANGLEMENT WITNESSES

Two-Tangle

This section describes how entanglement witnesses are calculated from our simulations, following the definitions of Ref. [25]. The two-tangle, which reflects the total entanglement carried by pairwise correlations, is derived from the pairwise correlations between two spins separated by a distance R , summed over the entire space. For the $S = 1/2$ Heisenberg chain, this becomes

$$\tau_2 = 8 \sum_{R \neq 0} \left[\max \left\{ 0, |g_R^{zz}| - \frac{1}{2} \left| \frac{1}{4} + g_R^{zz} \right| \right\} \right]^2, \quad (\text{S5})$$

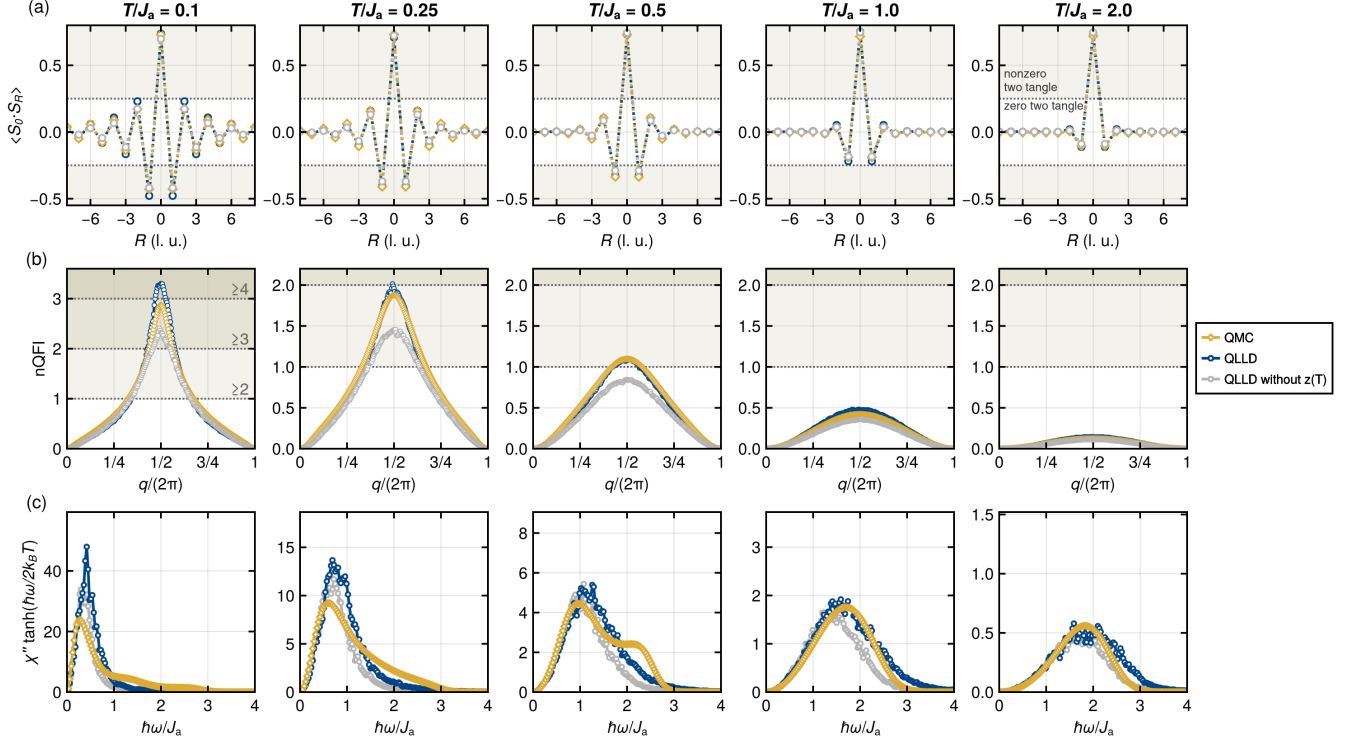


FIG. S2. (a) Real space spin-spin correlation $\langle \mathbf{S}_0 \cdot \mathbf{S}_R \rangle$ obtained in real space upon Fourier transform of QMC and LLD simulations. The distance R between the spins along the chain is given in lattice units. For $S = 1/2$, a value of $|\langle \mathbf{S}_0 \cdot \mathbf{S}_R \rangle| > 1/4 = S^2$ for $R \neq 0$ is necessary to obtain a non-zero two tangle. (b) Momentum space dependence of the normalized quantum Fisher information $f_Q(q)$. The grey horizontal lines and colored blocks indicate $f_Q > m$ which ensures the $(m + 1)$ multipartite entanglement. (c) QFI integrand at $q = \pi$. The temperature of each column is shown at the top of the column. Gold lines indicate QMC, blue lines are QLLD results, and grey lines show the LLD without $z(T)$ renormalization.

where $g_R^{zz} = \langle S_i^z S_{i+R}^z \rangle$ is the longitudinal spin-spin correlation. Given the translation symmetry of the problem, g_R^{zz} is related to the real-space spin-spin correlation function $\langle \mathbf{S}_0 \cdot \mathbf{S}_R \rangle$, Fig. S2(a), which is obtained from our simulations upon lattice Fourier transform and integration over energy. We observe $\langle \mathbf{S}_0 \cdot \mathbf{S}_R \rangle > 1/4 = S^2$ for nearest neighbor bonds and $k_B T/J_a < 1.0$, Fig. S2(b), which yields a non-zero two-tangle, see Eq. S5. As it focuses on spin correlations, we observe that the two-tangle is unaffected by the exchange scaling factor $z(T)$ in the QLLD simulation. This further suggests that the total bandwidth of magnetic excitations is irrelevant to the value of the two-tangle.

Quantum Fisher information

The quantum Fisher information (QFI) density is defined for a given momentum \mathbf{q} as:

$$f_Q(\mathbf{q}, T) = 4 \int_0^\infty d(\hbar\omega) \tanh\left(\frac{\hbar\omega}{2k_B T}\right) \times \left(1 - e^{-\hbar\omega/k_B T}\right) \mathcal{S}(\mathbf{q}, \hbar\omega, T) \quad (\text{S6})$$

where \mathcal{S} is the dynamical spin structure factor for given momentum \mathbf{q} and temperature T . Since the QFI is directly proportional to the strength of spin correlations, the QFI will be maximized where the intensity of DSSF is also strong. For the $S = 1/2$ Heisenberg spin chain case, the QFI density is calculated for $q = \pi$. For a general spin- S case in neutron scattering, bounds on the value of QFI can be expressed as

$$\text{nQFI} = \frac{f_Q}{12S^2} > m \quad (\text{S7})$$

where nQFI is called the normalized Quantum Fisher Information, which does not depend on the spin length. If the nQFI exceeds the integer m , the system has at least $m + 1$ entangled spins. Fig. S2(b) shows the momentum dependence of the nQFI

for selected temperatures, showing a good agreement between the nQFI density calculated with QLLD and QMC. Our QLLD simulations without exchange renormalization follow a similar temperature dependence as fully quantum-corrected LLD and QMC but with smaller values. This behavior trivially originates from the $\tanh(\hbar\omega/2k_B T)$ terms in the integrand of Eq.S7. This term de-emphasizes contributions from the lower energy part and emphasizes the higher energy part. Therefore, a simulation with an incorrect excitation bandwidth (here too small) will yield a smaller value for the nQFI. For completeness, the integrand of QFI is shown in Fig.S2(c).

Comparison with Literature Results

To check whether the entanglement witness values we extract from QLLD are reasonable, we compared our simulations with previous results on KCuF_3 . For the Fourier transform of the spin-spin correlation $S(q)$ in the momentum space, we used the data in $q = [0, 2\pi]$ and $\hbar\omega/J_a = [-4, 4]$. Tables I and II show the list of the two-tangle and QFI values calculated at a given temperature calculated in Ref. 23 and compared with our results. The temperature dependence of the two-tangle obtained by DMRG is matched by QMC and by our QLLD simulations. Moreover, the temperature dependence of normalized QFI obtained by QLLD is consistent with both DMRG and QMC. These results are summarized graphically in Fig. S3.

TABLE I. Comparison of two-tangle with the methods of Ref. [23]. The temperature was scaled to the exchange interaction of KCuF_3 of $J_a = 33.1$ meV.

$k_B T/J$	KCuF_3		$k_B T/J$	This Work	
	DMRG	INS data		QMC	QLLD
0.02	0.256	0.161	0.1	0.255	0.415
0.13	0.23	0.131	0.25	0.202	0.185
0.19	0.21	0.072	0.5	0.06	0.045
0.39	0.15	0.01	1.0	0.0	0.0
0.52	0.086	0.001	2.0	0.0	0.0
0.77	0.03	0.0			

TABLE II. Comparison of normalized Quantum Fisher Information with the methods of Ref. [23]. The temperature was scaled to the exchange interaction of KCuF_3 of $J_a = 33.1$ meV.

$k_B T/J$	KCuF_3		$k_B T/J$	This Work	
	DMRG	INS data		QMC	QLLD
0.02	3.81	3.72(14)	0.1	2.87	3.68
0.13	2.56	2.504(9)	0.25	2.88	2.03
0.19	2.14	1.92(14)	0.5	1.1	1.2
0.39	1.27	1.17(6)	1.0	0.42	0.54
0.52	0.96	0.9(5)	2.0	0.12	0.13
0.77	0.58	0.39(14)			

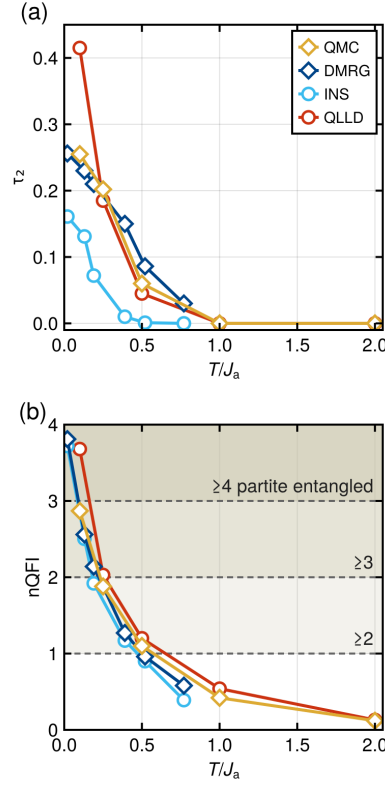


FIG. S3. (a) Temperature dependence of two-tangle τ_2 and (b) temperature dependence of normalized QFI from Density Matrix Renormalization Group calculations (Blue), Inelastic Neutron Scattering data on KCuF_3 (Cyan), Quantum Monte-Carlo (Gold) and quantum-corrected Landau-Lifshitz Dynamics (Red). The DMRG and INS results are taken from Ref. [23]

4. EFFECT OF QUANTUM CORRECTION ON LANDAU-LIFSHITZ DYNAMICS

Fig. S4 shows the effect of the quantum correction on the DSSF using Landau-Lifshitz dynamics. The first column shows the classical Landau-Lifshitz dynamics without correcting the DSSF. In this case, LLD does not obey the detailed balance $\mathcal{S}(\mathbf{q}, -\omega) = \exp(-\hbar\omega/k_B T)\mathcal{S}(\mathbf{q}, \omega)$ and the intensity of the high-energy part at the low temperature is weak. The second column is the LLD result with the quantum-to-classical (Q2C) energy-dependent correspondence (Ref. 17). After the Q2C correction, the DSSF follows the detailed balance, and the overall shape of the intensities looks similar to the QMC result, except for the bandwidth. The third correction is the moment rescaling, $\kappa(T)$ correction, which adjusts the spin length to match the quantum sum rule for each temperature. The moment rescaling, $\kappa(T)$ correction, gives excellent agreement with the QMC result in the high-temperature limit ($k_B T/J_a > 2.0$). Finally, exchange renormalization, $z(T)$ correction, is used to match the QMC data, resulting in an overall intensity and bandwidth that are almost consistent with each other, except for the continuum from the spinons in QMC data.

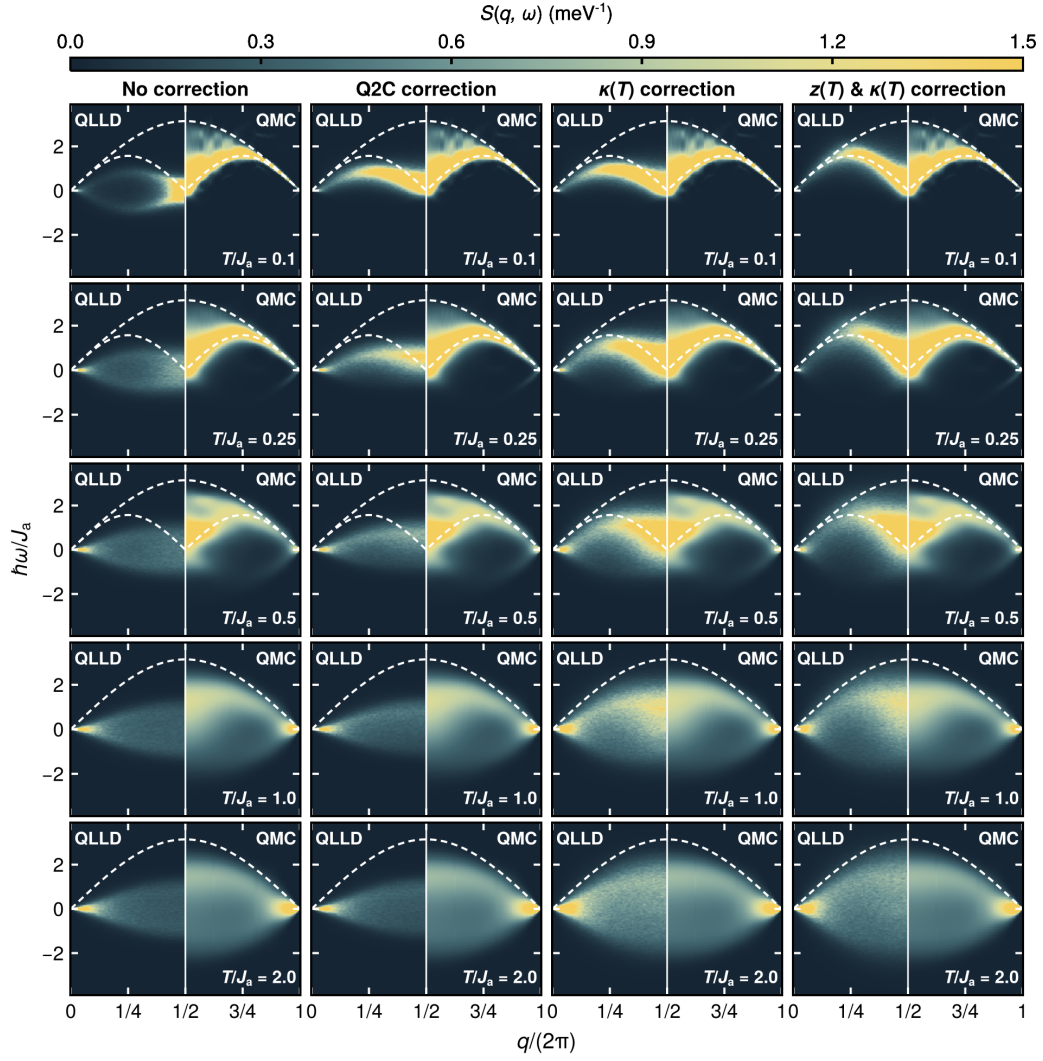


FIG. S4. Effect of quantum-to-classical correction in LLD simulation. Starting from the left, each column shows the LLD simulation without any correction, quantum-to-classical correspondence energy correction, quantum sum rule correction (i.e. $\kappa(T)$ moment rescaling), and exchange renormalization ($z(T)$), respectively. Each LLD calculation is directly compared with the QMC at the given temperatures.

5. SUPPLEMENTAL FIGURE FOR DYNAMICS IN APPLIED MAGNETIC FIELD

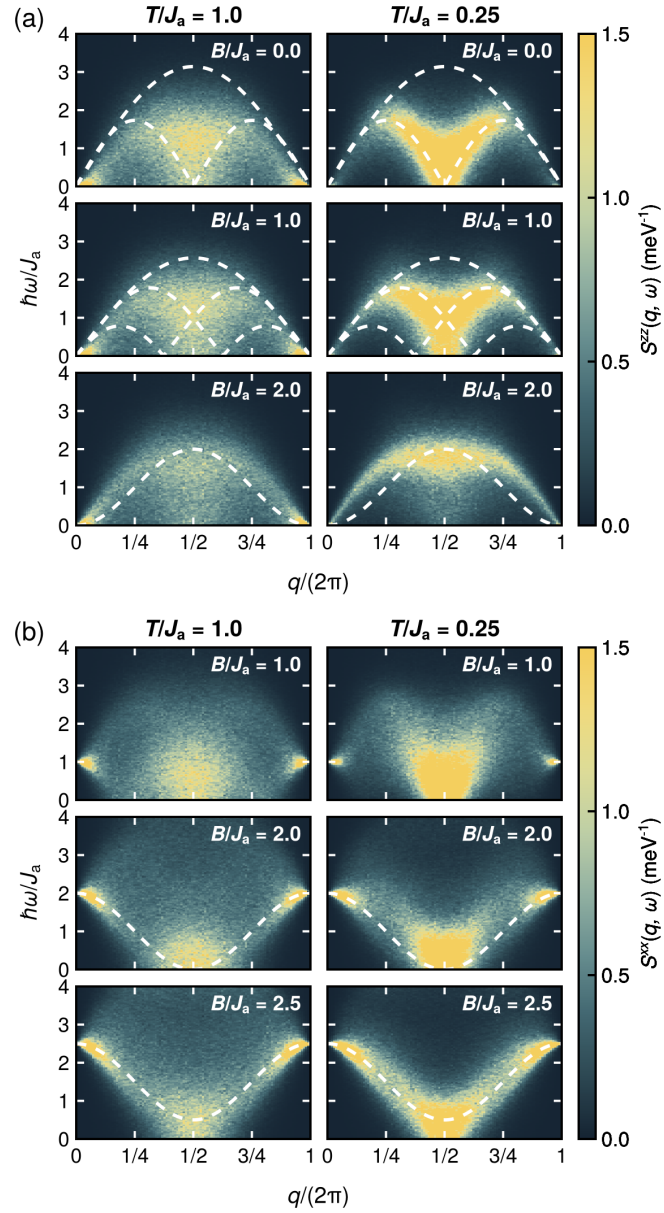


FIG. S5. Field and temperature dependence of DSSF by QMC and QLLD complementing the figure in the main text. (a),(b) indicates the longitudinal and transverse DSSF, respectively. White lines indicate the excitation boundary from the Muller ansatz at zero temperature.